 CMES, vol.86, no.1, pp.1-26, 2012

Steady Separated Flow Past Elliptic Cylinders Using a Stabilized Finite-Element Method

Subhankar Sen[1], Sanjay Mittal[2] and Gautam Biswas[1]

Abstract: The steady flow around elliptic cylinders is investigated using a stabilized finite-element method. The Reynolds number, Re, is based on cylinder major axis and free-stream speed. Results are presented for $Re \leq 40$ and $0^\circ \leq \alpha \leq 90^\circ$, where α is angle of attack. Cylinder aspect ratios, AR considered are 0.2 (thin), 0.5, 0.8 (thick) and 1.0. Results for the laminar separation Reynolds number, Re_s available in the literature are only for thin cylinder and exhibit large scatter. Also, very limited information is available for separation angle. The present study attempts to provide this data. In addition, issues concerning initial separation, such as location of separation and its evolution with α and Re, are studied. Symmetric cylinders are associated with a closed wake and consists of two attached eddies which appear at Re_s. Wake topology for asymmetric separation is proposed and compared with those of Smith (1983) and Dennis and Young (2003). The proposed topology differs significantly from the existing ones. For asymmetric cylinders, the wake is open and consists of an attached upper bubble and an unattached recirculation zone. The attached bubble appears at Re_s while the unattached zone appears at a larger Re. While symmetric separation initiates from base point, bubbles for asymmetric separation form near the trailing tip of thin and center of thick cylinders. For symmetric cylinders, the bubble elongates, approximately, linearly with Re. Irrespective of AR, Re_s exhibits non-monotonic variation with α.

Keywords: Elliptic cylinder, Stabilized finite-element, GMRES, Laminar separation, Wake topology.

1 Introduction

The flow past bluff bodies continues to remain an active area of research. The circular cylinder, flat plate normal to the flow and to some extent, square cylinders have received considerable attention. In contrast, there have been relatively fewer

[1] Department of Mechanical Engineering, Indian Institute of Technology Kanpur, India
[2] Department of Aerospace Engineering, Indian Institute of Technology Kanpur, India

efforts in understanding flow past cylinders of elliptical cross-section. The geometry of an elliptic cylinder is characterized by its aspect ratio, AR, defined as the ratio of lengths of its minor and major axes. Two extreme configurations of an ellipse are the flat plate ($AR = 0$) and a circular cylinder ($AR = 1$). Elliptic cylinders are widely used in heat exchangers owing to their superior performance compared to the circular cylinders (Khan, Culham and Yovanovich (2005)).

The onset of flow separation for a circular cylinder has been investigated by many researchers in the past (Taneda (1956a); Dennis and Chang (1970); Coutanceau and Bouard (1977)). The same has been carried out for a sphere by Taneda (1956b) and Pruppacher, Le Clair and Hamielec (1970) and for a square cylinder at zero incidence by Sen, Mittal and Biswas (2011). Recently, Sen, Mittal and Biswas (2009) numerically investigated the effects of blockage and boundary conditions on the critical Reynolds number for separation, Re_s, for a circular cylinder. The blockage is defined as the ratio of the cross-stream projection of the object, to the width of the experimental apparatus or computational domain. The steady flow characteristics of inclined elliptic cylinders have been studied earlier by Lugt and Haussling (1974), Park, Park and Hyun (1989), D'Alessio and Dennis (1994) and Dennis and Young (2003). For 45° inclined cylinders, Lugt and Haussling (1974) observed that the initial recirculatory region in the transient phase of numerical computations appears near the tips of thin but at the center for thick elliptic cylinders. It appears that the phenomenon of initial separation of laminar boundary layer from elliptic cylinders of various thickness and orientation has not received much attention. Also, very limited results (Masliyah and Epstein (1971); Weinbaum, Kolansky, Gluckman and Pfeffer (1976)) are available showing the variation of separation angle, θ_s for symmetric elliptic cylinders with Re. The separation Reynolds number, its dependence on angle of attack, α, and the origin as well as evolution with α of the location of initial separation are fundamental aspects of the flow. These issues are vital to the understanding of the initial flow separation from symmetric and asymmetric bluff bodies. A cylinder having either its major or minor axis aligned with the free-stream ($\alpha = 0^\circ$ or 90°, see Fig. 1) is termed 'symmetric'; the cylinder is 'asymmetric' otherwise. Large discrepancy is seen between the earlier predictions of Re_s values for certain cases. For instance, Dennis and Chang (1969) and Weinbaum, Kolansky, Gluckman and Pfeffer (1976) estimated Re_s to be ($\approx$) 200 and 100, respectively for $AR = 0.2$ and $\alpha = 0^\circ$. To the best of the knowledge of the current authors, only Park, Park and Hyun (1989) and Dennis and Young (2003) have presented results for Re_s for inclined thin cylinders. They, however, did not investigate the location of initial separation and its evolution with α. For a cylinder of $AR \approx 0.15$, Park, Park and Hyun (1989) presented a 'flow domain map' for $0^\circ \leq \alpha \leq 90^\circ$. This plot shows the values of Re that demarcate

the regimes of no separation and steady separation with an attached bubble. Based on numerical investigation, Dennis and Young (2003) presented, for the $AR = 0.2$ elliptic cylinder, a 'bifurcation diagram' in the $Re - \alpha$ plane (Fig. 9 of their paper) for $Re \leq 40$. Neither the results of Park, Park and Hyun (1989) or of Dennis and Young (2003) show the non-monotonicity in the $\alpha - Re$ profile which has been captured by the present results, perhaps, for the first time. In the present numerical investigation, the issues concerning initial separation are addressed through careful finite-element calculations performed using well resolved non-uniform meshes. A 'possible development' of the wake with α was proposed by Smith (1983) for a thin aerofoil. Subsequently, Dennis and Young (2003) presented results to show the wake topology for an $AR = 0.2$ cylinder. In the present study, wake topology is proposed for the steady flow. Differences between the present topology and the earlier ones are significant.

The early investigations in analyzing the flow past elliptic cylinders (Tomotika and Aoi (1953); Imai (1954)) were confined to very low Re. All these studies are based on analytical solution of Oseen's linearized equations of motion. The flow around elliptic cylinders in the $Re \leq 1$ regime was also studied by Yano and Kieda (1980), Shintani, Umemura and Takano (1983) and Sugihara-Seki (1993). One of the earliest numerical investigations for steady flow past elliptic cylinders was conducted by Dennis and Chang (1969). For $\alpha = 0^\circ$, they studied at $Re = 40$, the drag on elliptic cylinders of various aspect ratios. By employing finite-difference discretization of the steady streamfunction-vorticity ($\psi - \omega$) equations, Masliyah and Epstein (1971) investigated the steady flow past symmetrically oriented elliptic cylinders of aspect ratios ranging between 0.2 and 1. Results were presented for the pressure and vorticity distributions on the cylinder surface, drag coefficient, wake length and contours of streamfunction and vorticity. Lugt and Haussling (1974) employed finite-difference method for discretization of the unsteady $\psi - \omega$ equations and provided solutions at Re = 15, 30 and 200 for the flow past 45° inclined elliptic cylinders of $AR = 0.1$ and 0.2. Based on an approximate theory, Weinbaum, Kolansky, Gluckman and Pfeffer (1976) presented results for the separation angle of elliptic cylinders of various AR with major axis parallel to the incoming flow. Their $\theta_s - Re$ plot shows, a decrease in θ_s with decreasing AR while Re is held constant. Following a semi-analytical approach for the steady $\psi - \omega$ equations, D'Alessio and Dennis (1994) reported results for the flow and aerodynamic forces at $Re = 5$ and 20 for the inclined elliptic cylinder of $AR = 0.2$. The numerical experiments conducted by Dennis and Young (2003) are also based on semi-analytical method on the steady $\psi - \omega$ equations. An elliptic cylinder of $AR = 0.2$ was considered for Re range of $1-40$ and various α between 0° and 90°. Steady-state results were presented at $Re = 15$ and 30 also for $AR = 0.1$ and $\alpha = 45^\circ$. They reported

detailed results for the aerodynamic coefficients and defined various regimes of asymmetric separation. For the symmetric elliptic cylinders, Srinivasan (2006) recently proposed an analytical criterion for determining Re_s from the velocity field. For elliptic cylinders with major axes parallel to the incoming stream in unbounded flow ($\alpha = 0^\circ$), Faruquee, Ting, Fartaj, Barron and Carriveau (2007) recently studied at $Re = 40$, the effect of AR on the onset of separation, bubble dimensions and various flow parameters. They considered AR range of $0.3-1$ and concluded that no separation occurs at $Re = 40$ when AR <0.34. Sivakumar, Bharti and Chhabra (2007) reported extensive numerical results for the bubble length, drag, streamline pattern and surface pressure for symmetric elliptic cylinders of $AR = 0.2-1$. They investigated the power-law fluid flow (the power-law index = $0.2-1.8$) for an Re range of $0.01-40$.

The present study determines the critical Re for onset of separation, Re_s for the unbounded flow for various values of AR and α. The separation angle, θ_s at the critical Re is also estimated and detailed results are presented for the $\theta_s - Re$ variation. The effect of α and AR on the onset of flow separation is explored. The topology of steady wake is proposed for the inclined cylinders and compared with earlier results. To this end, elliptic cylinders of three different aspect ratios, i.e. 0.2 (thin), 0.5 and 0.8 (thick) are considered. For each AR, the angle of attack is varied from 0° to 90°, in steps of 15°. Results are also presented for $AR = 1$, i.e. circular cylinder. A stabilized Petrov Galerkin finite-element method with equal order bilinear interpolation for velocity and pressure is used.

The outline of the rest of the article is as follows. In Section 2, the governing equations for incompressible fluid flow are reviewed. The finite-element formulation involving stabilization parameters is presented in Section 3. The definition of the problem and finite-element mesh are described in Sections 4 and 5, respectively. Validation of the formulation, its implementation and the convergence studies are presented in Section 6. The main results are presented and discussed in Section 7. In Section 8, a few concluding remarks are made.

2 The governing equations

Let $\Omega \subset R^{n_{sd}}$ be the spatial domain, where $n_{sd} = 2$ is the number of space dimensions. The boundary of Ω is denoted by Γ and is assumed to be piecewise smooth. The spatial coordinates are denoted by $\mathbf{x} = (x, y)$. The equations governing the steady flow of an incompressible fluid of density, ρ, are:

$$\rho(\mathbf{u}\cdot\nabla\mathbf{u} - \mathbf{f}) - \nabla\cdot\boldsymbol{\sigma} = 0 \quad \text{on } \Omega, \tag{1}$$

$$\nabla\cdot\mathbf{u} = 0 \quad \text{on } \Omega. \tag{2}$$

Here $\mathbf{u} = (u, v)$, $\mathbf{f}$ and $\boldsymbol{\sigma}$ denote the fluid velocity, body force per unit volume and the Cauchy stress tensor, respectively. The stress is the sum of its isotropic and deviatoric parts:

$$\boldsymbol{\sigma} = -p\mathbf{I} + \mathbf{T}, \quad \mathbf{T} = 2\mu\boldsymbol{\varepsilon}(\mathbf{u}), \quad \boldsymbol{\varepsilon}(\mathbf{u}) = \tfrac{1}{2}((\boldsymbol{\nabla}\mathbf{u}) + (\boldsymbol{\nabla}\mathbf{u})^T) \tag{3}$$

where p, $\mathbf{I}$, μ and $\boldsymbol{\varepsilon}$ are the pressure, identity tensor, dynamic viscosity of the fluid and strain rate tensor, respectively. Both, the Dirichlet and Neumann-type boundary conditions are accounted for and are represented as

$$\mathbf{u} = \mathbf{g} \text{ on } \Gamma_g, \quad \mathsf{n} \cdot \boldsymbol{\sigma} = \mathbf{h} \text{ on } \Gamma_h, \tag{4}$$

respectively, where Γ_g and Γ_h are complementary subsets of the boundary Γ, n is its unit normal vector and $\mathbf{h}$ is the surface traction vector. The towing tank boundary condition has been successfully used earlier to simulate the unbounded flow past a circular cylinder (Sahin and Owens (2004); Sen, Mittal and Biswas (2009)). The same is used on the lateral walls of the domain in the present work. This boundary condition involves prescribed free-stream speed condition on the sidewalls and also on the upstream boundary. Figure 1a shows the boundary conditions used. No-slip boundary condition is applied on the surface of the cylinder. At the downstream boundary, a Neumann condition for velocity is specified that corresponds to stress-free condition.

3 The finite-element formulation

The spatial domain Ω is discretized into non-overlapping subdomains Ω^e, $e = 1, 2, ..., n_{el}$ where n_{el} is the number of elements. Let $\mathscr{S}_{\mathbf{u}}^h$ and $\mathscr{S}_p^h$ be the finite dimensional trial function spaces for velocity and pressure, respectively and the corresponding weighting function spaces are denoted by $\mathscr{V}_{\mathbf{u}}^h$ and $\mathscr{V}_p^h$. The stabilized finite-element formulation of the conservation Equations (1) and (2) is written as follows: find $\mathbf{u}^h \in \mathscr{S}_{\mathbf{u}}^h$ and $p^h \in \mathscr{S}_p^h$ such that $\forall \mathbf{w}^h \in \mathscr{V}_{\mathbf{u}}^h$, $q^h \in \mathscr{V}_p^h$

$$\begin{aligned}
&\int_\Omega \mathbf{w}^h \cdot \rho \left(\mathbf{u}^h \cdot \boldsymbol{\nabla}\mathbf{u}^h - \mathbf{f} \right) d\Omega + \int_\Omega \boldsymbol{\varepsilon}(\mathbf{w}^h) : \boldsymbol{\sigma}(p^h, \mathbf{u}^h) d\Omega + \int_\Omega q^h \boldsymbol{\nabla} \cdot \mathbf{u}^h d\Omega \\
&+ \sum_{e=1}^{n_{el}} \int_{\Omega^e} \frac{1}{\rho} \left(\tau_{\text{SUPG}} \rho \mathbf{u}^h \cdot \boldsymbol{\nabla}\mathbf{w}^h + \tau_{\text{PSPG}} \boldsymbol{\nabla} q^h \right) \cdot \left[\rho \left(\mathbf{u}^h \cdot \boldsymbol{\nabla}\mathbf{u}^h - \mathbf{f} \right) - \boldsymbol{\nabla} \cdot \boldsymbol{\sigma}(p^h, \mathbf{u}^h) \right] d\Omega^e \\
&+ \sum_{e=1}^{n_{el}} \int_{\Omega^e} \delta \boldsymbol{\nabla} \cdot \mathbf{w}^h \rho \boldsymbol{\nabla} \cdot \mathbf{u}^h d\Omega^e = \int_{\Gamma_h} \mathbf{w}^h \cdot \mathbf{h}^h d\Gamma.
\end{aligned} \tag{5}$$

In the variational formulation given by Equation (5), the first three terms and the right hand side constitute the Galerkin formulation of the problem. The first series

of element level integrals are the SUPG (streamline-upwind/Petrov-Galerkin) and PSPG (pressure-stabilizing/Petrov-Galerkin) stabilization terms added to the variational formulations of the momentum and the continuity equations, respectively. At high *Re*, in an advection dominated flow, the Galerkin formulation of the flow equations lead to node-to-node oscillations in the velocity field. This numerical instability is overcome by adding SUPG stabilization terms to the finite-element formulation. The SUPG formulation for convection dominated flows was introduced by Hughes and Brooks (1979) and Brooks and Hughes (1982). PSPG stabilization terms are added to the formulation to enable the use of equal order interpolation for velocity and pressure. Hughes, Franca and Balestra (1986) introduced the pressure stabilization methods in the context of Stokes flow and Tezduyar, Mittal, Ray and Shih (1992) generalized the method to finite Reynolds number flows. The second series of element level integrals are added for numerical stability at high Reynolds numbers. This is a least squares term based on the continuity equation. More details of the finite-element formulation can be found in Tezduyar, Mittal, Ray and Shih (1992).

4 Problem set-up

The elliptic cylinder with major axis of length 'a' is placed in a computational domain with rectangular outside boundary (see Fig. 1a). The flow is from left to right and the center of the cylinder coincides with the origin of the Cartesian coordinate system. The positive x axis is in the downstream direction. θ denotes the circumferential angle and is measured in a counterclockwise sense relative to the the negative x axis. The length of the minor axis is denoted by b and b/a represents the aspect ratio of the cylinder. The angle between the free-stream direction and major axis of the cylinder or the angle of attack, α is measured clockwise relative to the direction of incoming flow. Regardless of the value of α, the trailing tip of the cylinder is chosen as the base point. For all the computations, distance of the upstream and downstream boundaries from the cylinder center are $L_u = 80a$ and $L_d = 120a$, respectively. The sidewalls are equidistant from the cylinder center; the distance between the sidewalls, H, is $100a$ for all the computations. This set-up results in a blockage of 0.01 for $\alpha = 90^\circ$. The blockage is smaller than 0.01 for lower values of α. The Reynolds number, Re $(= Ua/\nu)$, is based on the major axis and free-stream speed. The moment exerted by fluid on the cylinder is calculated at the center of the cylinder. The drag (C_d), lift (C_l) and moment (C_m) coefficients

(Fig. 1b shows the positive sign convention) are defined as

$$C_d = \frac{1}{\frac{1}{2}\rho U^2 a}\int_{\Gamma_{cyl}} \mathsf{n}_\mathsf{x}\cdot\boldsymbol{\sigma}d\Gamma, \quad C_l = \frac{1}{\frac{1}{2}\rho U^2 a}\int_{\Gamma_{cyl}} \mathsf{n}_\mathsf{y}\cdot\boldsymbol{\sigma}d\Gamma,$$
$$C_m = \frac{1}{\frac{1}{2}\rho U^2 a^2}\int_{\Gamma_{cyl}} (\mathsf{n}\cdot\boldsymbol{\sigma})\times \mathsf{r}d\Gamma. \tag{6}$$

Here n_x and n_y are the x and y components, respectively of the unit vector n normal to the cylinder boundary, Γ_{cyl} and r is the radius vector of any arbitrary point located on the cylinder surface measured from the center of cylinder.

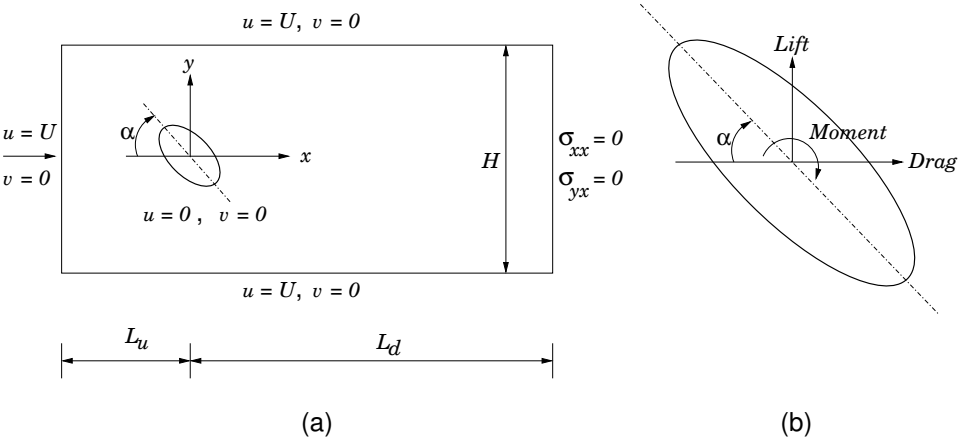

Figure 1: Steady flow past a stationary elliptic cylinder inclined at an angle α ($0^\circ \leq \alpha \leq 90^\circ$) to the free-stream: (a) problem definition, (b) the aerodynamic forces and moment acting on the cylinder. Clockwise moment is considered positive.

5 The finite-element mesh

A representative finite-element mesh, used for computations for $\alpha = 45^\circ$ and $AR = 0.2$ is shown in Fig. 2. The number of nodes and elements are 120626 and 119768, respectively. The mesh has been constructed by combining five blocks; a central square block containing the cylinder and four neighbouring rectangular blocks one each, located to the left, right, top and bottom of the central block. The number of nodes on the cylinder surface or any other circumferential grid line is N_t (= 464) and the radial thickness of the first layer of elements located on the cylinder surface is, h_1^r (= $0.0005a$).

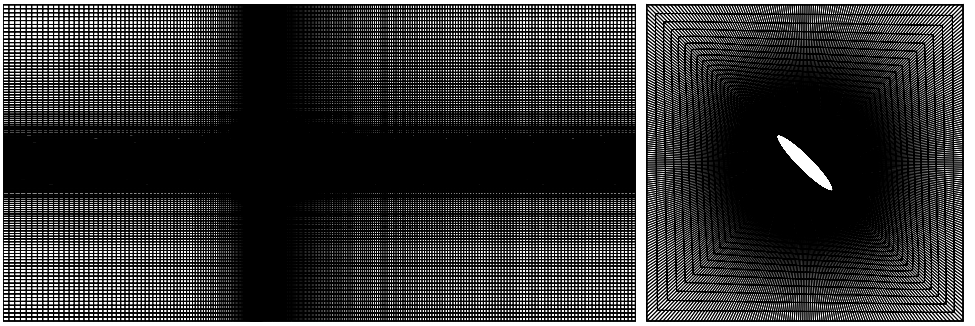

(a) (b)

Figure 2: Steady flow past an elliptic cylinder of $AR = 0.2$: (a) finite-element mesh corresponding to $\alpha = 45^\circ$, consists of 120626 nodes and 119768 bilinear quadrilateral elements, (b) close-up of the central square block containing the cylinder.

6 Validation of method and convergence of results

6.1 Comparison with the earlier studies

Table 1: Steady flow past a symmetric elliptic cylinder of $AR = 0.5$ for $5 \leq Re \leq 40$: comparison of the predicted total drag coefficient and its components with those reported by Sivakumar, Bharti and Chhabra (2007).

α	Re	Sivakumar, Bharti and Chhabra (2007)			Present		
		C_{dp}	C_{dv}	C_d	C_{dp}	C_{dv}	C_d
0°	10	0.7799	1.3439	2.1238	0.7903	1.3402	2.1305
0°	40	0.4447	0.5867	1.0314	0.4488	0.5840	1.0328
90°	10	1.9253	0.7945	2.7198	1.9640	0.7850	2.7490
90°	40	1.2289	0.3278	1.5567	1.2443	0.3228	1.5671

To ascertain the validity of the finite-element formulation as well as its implementation, the computed aerodynamic coefficients are compared with those reported by the earlier numerical studies. Shown in Tab. 1 is a comparison of the predicted C_{dp}, C_{dv} and C_d with the recent numerical results of Sivakumar, Bharti and Chhabra (2007) for a symmetric cylinder of $AR = 0.5$. C_{dp} and C_{dv} respectively represent the pressure and viscous components of C_d. For each Reynolds number considered, the comparison reveals excellent agreement.

Table 2: Steady unbounded flow at $Re = 15$ and 30 past an elliptic cylinder of $AR = 0.1$ for $\alpha = 45^\circ$: comparison of the predicted aerodynamic force and moment coefficients with the earlier numerical studies.

Studies	Re	C_d	C_l	C_m
Dennis and Young (2003)	15	1.8700	1.0650	0.2912
Alben (2008)	15	1.8730	1.0510	
Present	15	1.8984	1.0788	0.3051
Lugt and Haussling (1974)	30	1.4300	0.9350	0.2525
Dennis and Young (2003)	30	1.4060	0.9410	0.2444
Alben (2008)	30	1.4110	0.9310	
Present	30	1.4252	0.9431	0.2556

For $AR = 0.1$ and $\alpha = 45^\circ$, Tab. 2 demonstrates that the predicted aerodynamic force and moment coefficients at $Re = 15$ and 30 compare favourably with those reported by Lugt and Haussling (1974) and Alben (2008) (maximum difference is about 2.5% in C_l with Alben (2008) at $Re = 15$). While the computed aerodynamic forces are close (maximum difference about 1.5%) to those reported by Dennis and Young (2003), a maximum difference of about 4.5% is observed in the moment coefficient.

Table 3 compares at $Re = 20$, the predicted aerodynamic coefficients of an inclined elliptic cylinder of $AR = 0.2$ with other numerical results available in the literature. Overall, the comparison reveals a satisfactory agreement between the present and earlier predictions for the range of α considered.

For various α, the aerodynamic coefficients obtained from the present simulations for a thin elliptic cylinder ($AR = 0.2$) at $Re = 40$ are compared in Tab. 4 with those documented by the earlier numerical studies. The predicted results are very close to those reported by Dennis and Young (2003) for small α. However, as α increases beyond 20°, the discrepancies between the two sets of data increase. The comparison of C_d with the recent predictions by Sivakumar, Bharti and Chhabra (2007) on the other hand, reveals excellent agreement for both of $\alpha = 0^\circ$ and 90°. At the same Re, Masliyah and Epstein (1971)) reported $C_d = 1.814$ for the $AR = 0.2$ cylinder oriented normal to the free-stream. As seen from Tab. 4, this value shows considerable divergence with the present prediction of 1.6351.

6.2 Effect of the streamwise extent of the domain

Details on the effect of streamwise extent of the domain on flow characteristics can be found in Sen (2010).

Table 3: Steady flow past an inclined elliptic cylinder of $AR = 0.2$: comparison of the predicted total drag and lift coefficients with earlier numerical efforts at $Re = 20$. The abbreviations used are: D'A-D, D'Alessio and Dennis (1994); D-Y, Dennis and Young (2003); S, Sivakumar, Bharti and Chhabra (2007); A, Alben (2008).

α	D'A-D		D-Y		S		A		Present	
	C_d	C_l	C_d	C_l	C_d	C_l	C_d	C_l	C_d	C_l
0°	1.1690	0	1.1690	0	1.1680	0			1.1503	0
20°	1.3050	0.7510	1.2960	0.7410			1.2930	0.7420	1.2850	0.7334
40°	1.6200	0.9490	1.6020	0.9470			1.6010	0.9320	1.5905	0.9222
60°	1.9310	0.7060	1.9110	0.7060			1.9030	0.6890	1.8891	0.6819
80°	2.1160	0.2560	2.0930	0.2570			2.0800	0.2490	2.0643	0.2462
90°	2.1400	0	2.1190	0	2.0802	0			2.0873	0

6.3 Mesh convergence

To test the mesh independence of computed results, several meshes with increasing spatial resolution are utilized to compute the flow past an $AR = 0.2$ cylinder at $Re = 10$ and 40. The angle of attack considered is, $\alpha = 45°$. For each mesh, $L_u = 80a$ and $L_d = 120a$. Out of the many meshes studied for mesh convergence, Tab. 5 lists the relevant parameters for meshes M1 and M2. The number of nodes and elements in M2 are roughly twice of those used in M1. Tab. 5 also summarizes the results of mesh convergence study. The results suggest that the aerodynamic coefficients are almost constant for mesh M1 and beyond. Therefore, mesh M1 is used for the present computations.

7 Results

The steady and laminar unbounded flow around stationary elliptic cylinders has been investigated for three parameters: Reynolds number ($Re \leq 40$), aspect ratio (AR = 0.2, 0.5, 0.8 and 1) and angle of attack ($0° \leq \alpha \leq 90°$). The element level matrix and vector entries have been computed by employing the 2×2 points Gauss-Legendre quadrature formula. The linearized algebraic equations of fluid flow have been solved by a matrix-free implementation of GMRES or Generalized Minimal RESidual method of Saad and Schultz (1986) in conjunction with diagonal pre-conditioner to accelerate the convergence rate.

Table 4: Steady flow at $Re = 40$ past an inclined elliptic cylinder of $AR = 0.2$: comparison of the predicted aerodynamic coefficients with the earlier numerical studies. The abbreviation S stands for Sivakumar, Bharti and Chhabra (2007)

α	Dennis and Young (2003)			S		Present		
	C_d	C_l	C_m	C_d	C_l	C_d	C_l	C_m
0°	0.7890	0	0	0.7860	0	0.7753	0	0
10°	0.8180	0.4190	0.1360			0.8085	0.4194	0.1285
20°	0.9040	0.7170	0.2287			0.9021	0.7116	0.2174
30°	1.0510	0.8830	0.2647			1.0372	0.8306	0.2523
40°	1.2290	0.9000	0.2555			1.1885	0.8156	0.2451
60°	1.5920	0.6780	0.1747			1.4597	0.5778	0.1679
80°	1.8410	0.2550	0.0612			1.6622	0.2060	0.0573
90°	1.8760	0	0	1.6319	0	1.6351	0	0

Table 5: Steady unbounded flow past a 45° inclined elliptic cylinder of $AR = 0.2$: effect of the mesh resolution on the characteristics of the flow. The other parameters for the meshes are $L_u = 80a$, $L_d = 120a$ and $h_1^r = 0.0005a$.

Mesh	Nodes	Elements	N_t	C_d		C_l		C_m	
				$Re = 10$	40	10	40	10	40
M1	120626	119768	464	2.3052	1.2631	0.9891	0.7757	0.3083	0.2314
M2	240954	239740	616	2.3043	1.2626	0.9882	0.7755	0.3080	0.2312

7.1 Development of the wake with Re and α

The symmetrically and asymmetrically oriented cylinders contain an even number of points on the surface where the vorticity vanishes ($\omega = 0$). These are points of attachment and separation that are alternately placed on the cylinder (Lighthill (1963)). An unseparated flow is characterized by the presence of two such points on the cylinder, namely, the forward and rear stagnation points implying attachment and separation, respectively. The steady separation of laminar boundary layer is marked with the appearance of a tiny separation bubble on the cylinder surface that involves two additional zero-vorticity points.

The development of the steady wake of a circular as well as elliptic cylinders inclined at $\alpha = 45°$, with Re, is studied. The streamlines for the steady flow are shown in Fig. 3 for $5 \leq Re \leq 40$ and $0.2 \leq AR \leq 1$. The flow in this figure is observed to separate for $Re = 20$ and 40 but is attached for $Re = 5$. For the sep-

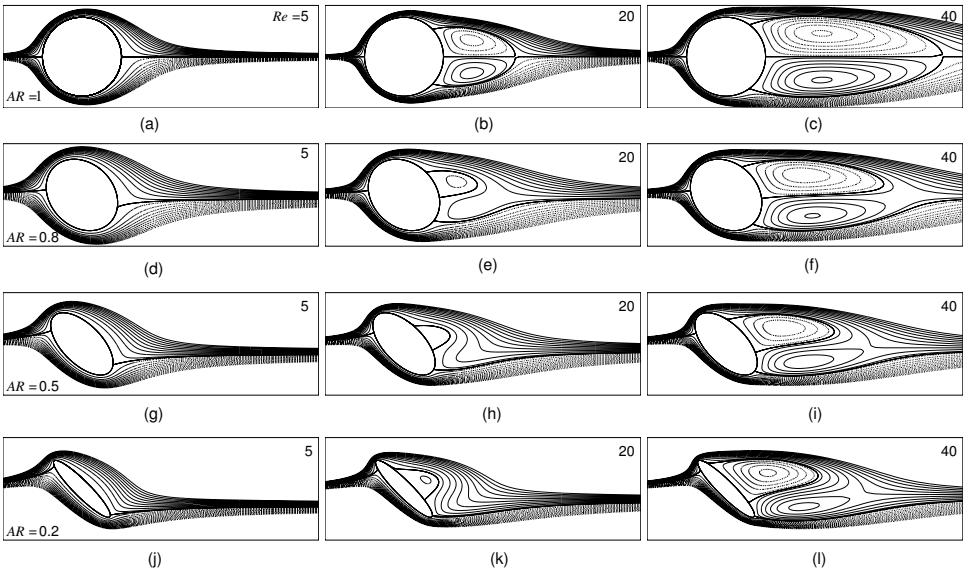

Figure 3: Steady unbounded flow past 45° inclined elliptic cylinders at $Re = 5-40$: the streamline contours for $AR = 1$, (a-c); 0.8, (d-f); 0.5, (g-i) and 0.2, (j-l).

arated flow, four points with zero-vorticity are seen on the cylinder (Figs. 3(b,e), for example). The attached bubble of a circle (Figs. 3(b,c)) is symmetric about the x axis (wake centerline) and contains two counterrotating recirculation zones. The wake is closed and a well defined wake stagnation point identified as an inviscid saddle point (Perry, Chong and Lim (1982)), marks the streamwise extremity of the wake. With increasing Re, the bubble elongates both in the longitudinal and transverse directions. The attached bubble of asymmetric cylinders (Figs. 3(e,h,k)) in contrast, contains a single recirculation zone. As Re increases, the bubble grows larger and subsequently an isolated recirculation zone with opposite sense of recirculation, appears below the bubble (Figs. 3(f,i,l)). Hence, the two recirculation zones do not appear at the same Re. Appearance of the unattached eddy at $Re > Re_s$ for inclined cylinders, marks a fundamental difference with the boundary layer separation from symmetric cylinders where the twin vortices appear essentially at the same Re_s. The attached bubble for the $AR = 0.5$ cylinder, for instance, appears first at $Re = 11.89$ while the isolated zone appears at an Re between 25 and 26. A pack of streamlines adjacent to and above the dividing or forward stagnation streamline closely follows the contour of the attached bubble and subsequently bend towards the downstream. A highly curved flow passage forms between the attached and unattached recirculation regimes. This flow passage is referred to as the 'alleyway'

by (Perry, Chong and Lim (1982)) in conjunction with the two-dimensional unsteady flow past a circular cylinder. The downstream extremity of the 'developed wake' of an asymmetric cylinder is marked by an inviscid saddle point (point M in Fig. 5b). The wake is 'open' in the sense that the viscous saddle points on the cylinder (the forward stagnation and attachment points, for example) and the inviscid saddle point in the wake are not connected by separation streamlines or separatrices (Perry, Chong and Lim (1982)).

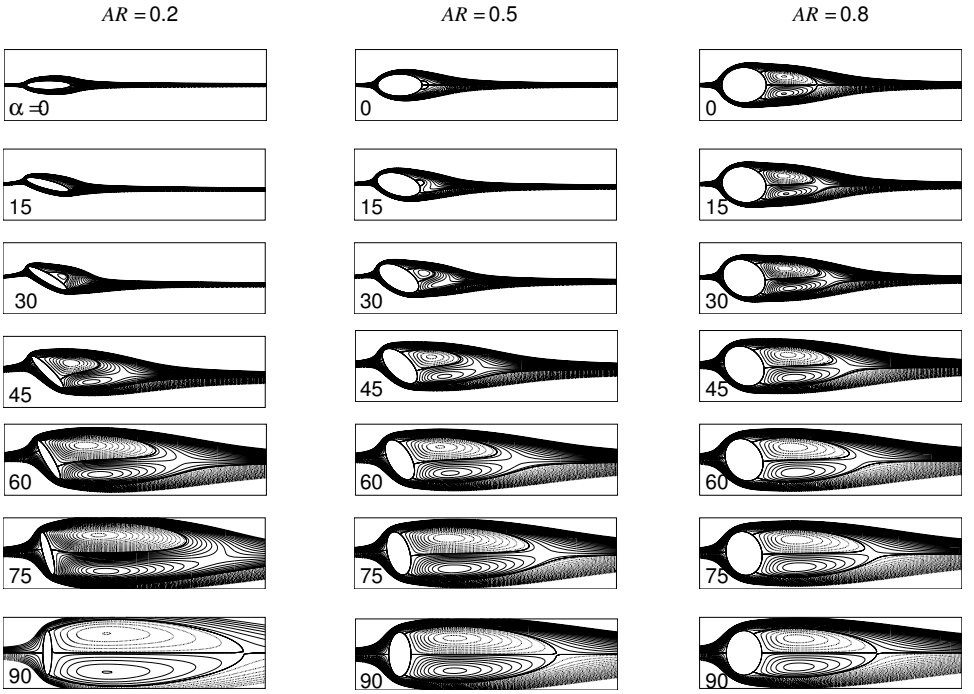

Figure 4: Steady unbounded flow past elliptic cylinders at $Re = 40$ and various angles of attack between 0° and 90°: the first, second and third columns show the streamlines for $AR = 0.2$, 0.5 and 0.8, respectively.

Figure 4 shows at $Re = 40$, the steady wake of cylinders of various AR and different values of α. The aspect ratios considered are 0.2, 0.5 and 0.8 while the angle of attack varies between 0° and 90°. For separated flow, a symmetric wake comprising of two attached recirculation regimes are observed for all AR when $\alpha = 0^\circ$ and 90°. However, the wake is asymmetric and open for other values of α. For each AR, the overall size of the wake increases with increasing α and reaches the maximum

when $\alpha = 90^\circ$. As seen from the third column of Fig. 4, the attached and unattached recirculation zones of a thick cylinder for each α are of comparable size in both the streamwise and cross-stream directions. As AR decreases, the effect of alleyways become stronger and inhibit the transverse expansion of the isolated zone leading to smaller width compared to the attached bubble. The present results indicate that it is always the upper bubble that remains attached to the asymmetrically oriented cylinder while the lower bubble remains unattached. As long as the cylinder is oriented asymmetrically, no transition is observed in this unique wake pattern.

7.2 The wake topology and surface vorticity

The topological phase plot in Fig. 4 of Brons, Jakobsen, Niss, Bisgaard and Voigt (2007) in relation to a circular cylinder, covers the possible streamline patterns for both the symmetric and asymmetric wakes. The plot is valid for geometries that can be generated from a circle (Aref, Brøns and Stremler (2007)). Our predicted streamline patterns are contained in the phase plot of Brons, Jakobsen, Niss, Bisgaard and Voigt (2007). The structure of the steady wake of a symmetric elliptic cylinder is shown schematically in Fig. 5a for $\alpha = 0^\circ$. The bubble is closed and consists of two symmetric, counterrotating recirculation zones. The key geometrical parameters characterizing the bubble are the bubble/eddy length, L and separation angle, θ_s. The convention for measuring L and θ_s is shown in the figure.

Based on the predicted streamline patterns in Section 7.1, our proposed topology of the 'developed wake' of an inclined elliptic cylinder is shown in Fig. 5b. R′ in this figure is the base point. As opposed to the closed wake for a symmetric cylinder, the 'developed' wake of an inclined cylinder is 'open' and consists of an attached upper separation bubble and an unattached recirculation zone located below the bubble. The attached bubble bounded by the separatrix SR consists of only one recirculation zone. Unlike point G for a symmetric cylinder, the saddle-type stagnation point M in the wake of an inclined cylinder does not form due to interaction of the separatrices emanating from the points S and Q and hence, is not connected to the cylinder. In Fig. 5, P and R are attachment points while Q and S represent separation points. Note that the rear stagnation point of a symmetric cylinder (point R, Fig. 5a) is an attachment point while for an inclined cylinder (point Q, Fig. 5b), this is a separation point.

Smith (1983) proposed a schematic demonstrating the 'possible development' of the wake with α (see the first column of Fig. 6). According to this schematic, a single attached eddy forms at low α. This eddy gets stronger with increasing α. Beyond a certain α, a weak and unattached eddy appears below the attached eddy. The wake is predicted to achieve a closed state on further increase in α

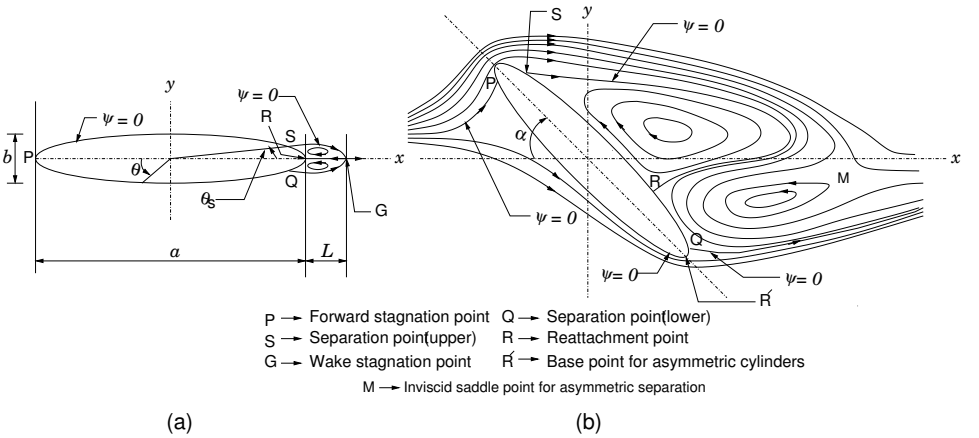

Figure 5: Schematic representation of the wake topology when the major axis of the elliptic cylinder is (a) parallel to the incoming stream, i.e. $\alpha = 0^\circ$ and (b) oriented at an arbitrary α.

(Figure D of the first column of Fig. 6). Note that this phenomenon is proposed to occur at an α much lower than 90°. He also proposed an alternate topology with a single predominant eddy. However, no schematic of the flow was presented for this proposal. Later, Dennis and Young (2003) presented the wake topology for $AR = 0.2$ at $Re = 40$ (second column of Fig. 6). The wake topology from the present computations (third column of Fig. 6) is in stark contrast with those proposed by Smith (1983). The topology suggested by the present computations neither predicts a closed wake for asymmetric separation nor the presence of a single predominant eddy. For various α, Fig. 6 compares, the predicted wake topology at $Re = 40$ with those reported by Dennis and Young (2003) for $AR = 0.2$. The comparison reveals several distinctive features of the streamline topology as obtained by these two sets of computations. The streamline patterns for the two studies are qualitatively similar for $\alpha \leq 30^\circ$. However, significant differences are observed for large α. The results of Dennis and Young (2003) show that for $\alpha < 57^\circ$, the upper bubble is attached and the lower one is detached from the body. This is seen for $\alpha = 40^\circ$ in second column of Fig. 6. A transition in the topology of the bubbles in the wake takes place at $\alpha \approx 57^\circ$. For $\alpha \approx 57^\circ$, both bubbles are attached to the cylinder. For $\alpha > 57^\circ$, the upper one detaches and the lower one is attached. This can also be observed from the second column of Fig. 6, for $\alpha = 70^\circ$, if one looks at it closely. Our computations do not exhibit any such transition. As shown in the third column of Fig. 6, the upper bubble is attached while the lower one is detached from the cylinder for $\alpha \geq 45^\circ$. A symmetric pair of attached bubbles is observed

for $\alpha = 90^\circ$. The size of the recirculation zone is underpredicted by Dennis and Young (2003).

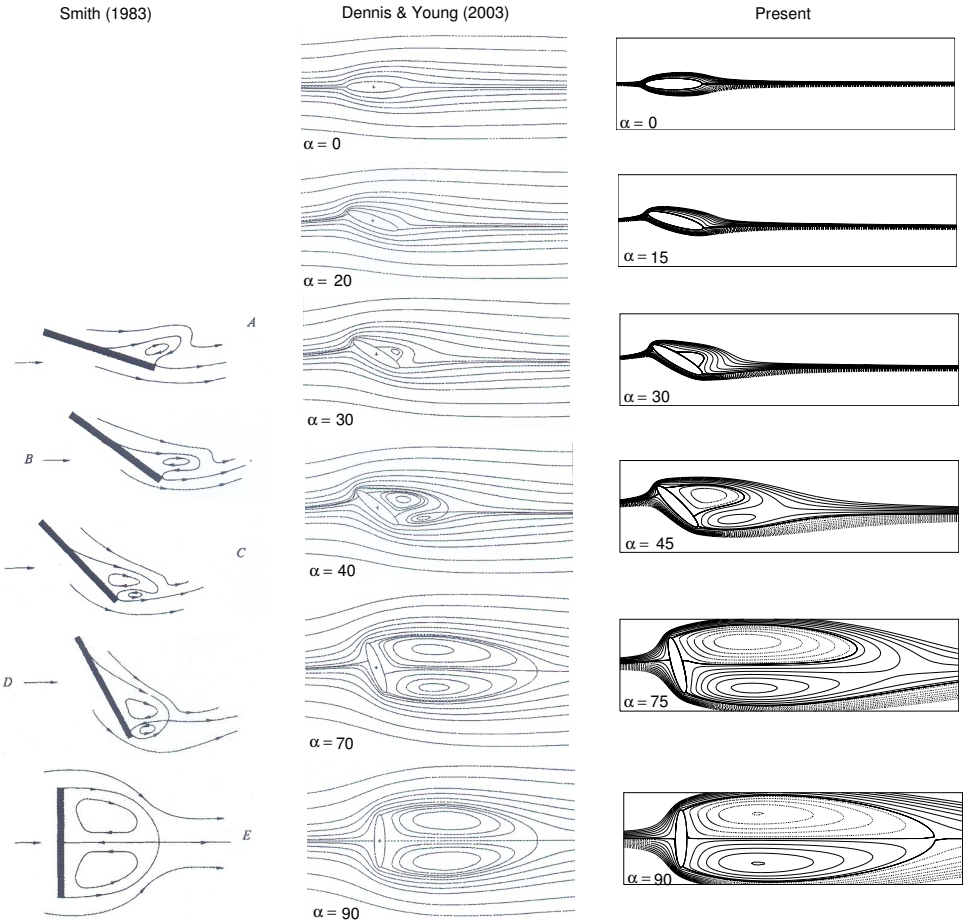

Figure 6: Comparison of the streamline topology reported by Dennis and Young (2003) (reproduced from Figure 7 of their paper) and the present effort for $AR = 0.2$ and $Re = 40$. The wake topology proposed by Smith (1983) for a thin aerofoil is also shown in the first column (reproduced from Figure 9 of Smith (1983)). For the proposal of Smith (1983), values of Re and α are not specified.

Figure 7 shows the vorticity distribution on the surface of the cylinder. The vorticity distribution along the surface of a symmetric cylinder reveals antisymmetry about the $\theta = 180^\circ$ location. The vorticity vanishes at the stagnation points, i.e. $\theta = 0^\circ$ (or 360°) and 180°. The other zero-vorticity points, if they exist, represent the upper

and lower separation points. For $Re = 40$, Figs. 7a ($\alpha = 0^\circ$) and 7c ($\alpha = 90^\circ$) demonstrate these features for $AR = 0.2$ and 0.5. The antisymmetry of the $\omega - \theta$ profiles is lost when a cylinder is oriented asymmetrically as seen from Fig. 7b for a representative α of 45°. Fig. 7b also shows for $AR = 0.2$, the relative positions of the various separation-attachment points on the $\omega - \theta$ curve. As expected for single attached bubble, the portion of the curve between points S and R indicates that vorticity within the bubble is *always* of same sign along the surface of asymmetric cylinders.

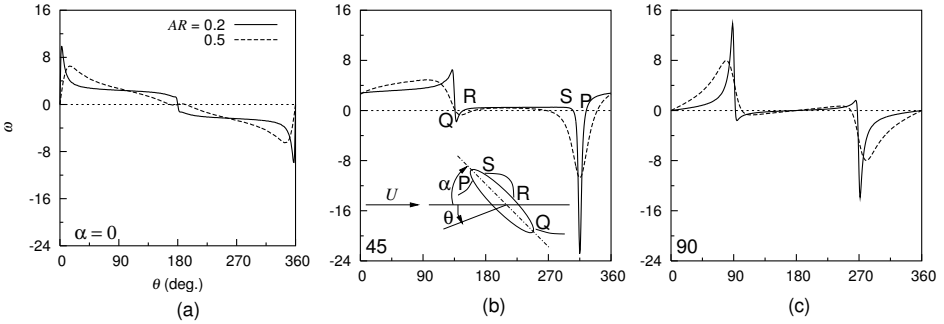

Figure 7: Steady unbounded flow past elliptic cylinders at $Re = 40$: the surface vorticity distribution for cylinders of $AR = 0.2$ and 0.5 for $\alpha =$ (a) 0°, (b) 45° and (c) 90°. Figure 7b shows the location of separation-attachment points on the cylinder surface for a representative $AR = 0.2$ and $\alpha = 45^\circ$.

7.3 The separation Reynolds number

To determine Re_s for circular and square cylinders, Sen, Mittal and Biswas (2009, 2011) utilized the linearity property of eddy length with Re. For unbounded flow, the predicted value of Re_s for the circle is 6.29 (Sen, Mittal and Biswas (2009)) and for the square 1.15 (Sen, Mittal and Biswas (2011)). The Re_s predicted for a circular cylinder shows an exact convergence with the recent prediction of Brons, Jakobsen, Niss, Bisgaard and Voigt (2007). Sen, Mittal and Biswas (2009) also utilized the analytical criterion of Srinivasan (2006) to predict Re_s for the circular/symmetric elliptic cylinders. At Re_s, this criterion specifies a zero value of $\frac{\partial^2 u}{\partial x^2}$ at the base point. Excellent agreement between both sets of predictions was seen for a wide range of blockage. In the present study, we determine Re_s for the symmetric cylinders using both the eddy length and $\frac{\partial^2 u}{\partial x^2} = 0$ criteria. Fig. 9 in Section 7.4 shows linear $L - Re$ variation. For a circular cylinder in the unbounded medium, the present study also yields $Re_s = 6.29$. The Re_s for asymmetric cylin-

ders are determined from the plots of surface vorticity distribution. Onset of laminar boundary layer separation is marked by the appearance of a tiny attached bubble aft the cylinder (see Section 7.1). The separation *Re* is therefore determined from a criterion requiring zero reattachment length SR (see Fig. 5b) along the cylinder surface. Starting from a guessed *Re* that gives a small value of SR (see Fig. 7b), the Reynolds number is progressively reduced till the limit of no attached bubble is reached. The Reynolds number immediately above the 'no bubble' *Re* is chosen as Re_s.

Table 6: Re_s obtained for the steady unbounded flow past elliptic cylinders of $0.2 \leq AR \leq 0.8$. The Re_s values within parentheses for $\alpha = 0^\circ$ and 90° are obtained by using the criterion proposed by Srinivasan (2006).

α	AR	Re_s	AR	Re_s	AR	Re_s
0°	0.2	184.75 (187.51)	0.5	25.88 (26.03)	0.8	9.90 (9.94)
5°	0.2	208.90	0.5	31.12	0.8	11.08
15°	0.2	81.28	0.5	28.71	0.8	11.66
30°	0.2	24.33	0.5	18.84	0.8	10.95
45°	0.2	11.07	0.5	11.89	0.8	9.46
60°	0.2	6.06	0.5	7.90	0.8	7.93
75°	0.2	3.42	0.5	5.44	0.8	6.58
90°	0.2	1.05 (1.06)	0.5	3.02 (3.04)	0.8	4.99 (5.01)

The values of Re_s obtained by using the aforesaid criteria are listed in Tab. 6 for elliptic cylinders of $AR = 0.2 - 0.8$ for various α. The Re_s obtained for $\alpha = 0^\circ$ and 90° by using the criterion of Srinivasan (2006) are shown in parentheses. Very close agreement is observed with those obtained using the bubble length criterion. The maximum difference between the two sets of results is 1.5%, approximately. With decreasing AR, Tab. 6 indicates a monotonic increase of Re_s for $\alpha = 0^\circ$ and a monotonic decrease of Re_s for $\alpha = 90^\circ$. The later trend was earlier suggested by Batchelor (1967) and also noted by Park, Park and Hyun (1989). A cylinder of given AR leads to much earlier separation of flow (smaller Re_s) when $\alpha = 90^\circ$ than when $\alpha = 0^\circ$. For $AR = 0.2$ and $\alpha = 90^\circ$, Dennis and Young (2003) determined $Re_s = 1.45$. This value shows considerable divergence with the currently predicted Re_s value of 1.05. The overprediction of Re_s by Dennis and Young (2003) is an outcome of the underprediction of bubble length by them (see Section 7.4). Dennis and Chang (1969) estimated Re_s close to 200 for the $AR = 0.2$ cylinder at $\alpha = 0^\circ$. This value also shows significant discrepancy with the presently predicted value of Re_s (= 184.75). Weinbaum, Kolansky, Gluckman and Pfeffer (1976) estimated the

corresponding onset *Re* to be approximately 100 which shows too large a divergence with the present prediction and those by Dennis and Chang (1969).

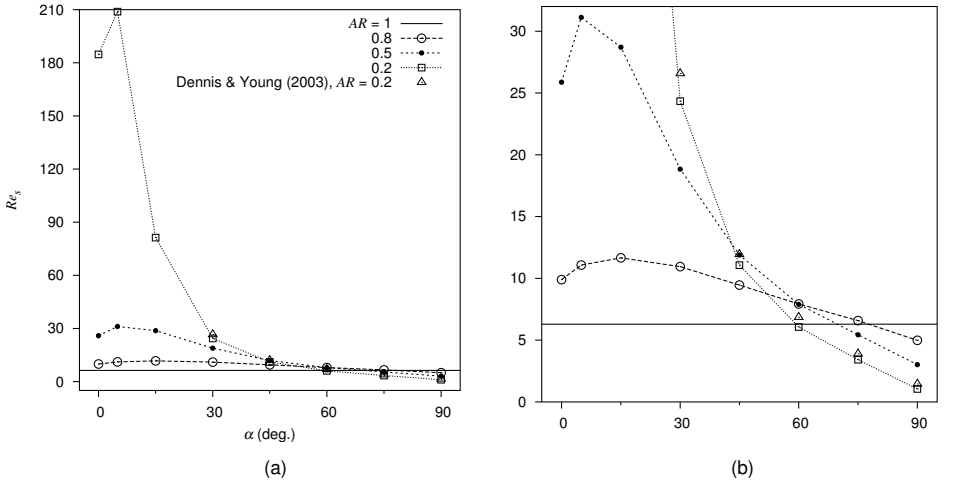

Figure 8: Steady unbounded flow past elliptic cylinders of aspect ratios 0.2, 0.5, 0.8 and 1: (a) dependence of Re_s on α, (b) enlarged view of (a). Re_s predicted by Dennis and Young (2003) for $AR = 0.2$, $\alpha \geq 30^\circ$ are also plotted.

The results summarized in Tab. 6 are presented in Fig. 8 showing the dependence of Re_s on α. The predicted separation *Re* for a circular cylinder as well as those obtained by Dennis and Young (2003) for $AR = 0.2$, $\alpha \geq 30^\circ$ are also plotted. Fig. 8 demonstrates a non-monotonic $Re_s - \alpha$ relationship for elliptic cylinders of $AR < 1$. With increasing α, a rise in Re_s followed by a decay is observed. This is the first time that such an $Re_s - \alpha$ relationship displaying non-monotonicity is being reported. Higher the *AR* of non-circular cylinders, lower is the Re_s for $\alpha < 45^\circ$. The trend reverses for $\alpha > 45^\circ$. The 'flow domain map' of Park, Park and Hyun (1989) shows no regime of non-monotonicity when their Equation 14 characterizing the steady separation is plotted. Also, the bifurcation diagram presented by Dennis and Young (2003) is limited to $Re \leq 40$ and hence could not capture the non-monotonic $Re_s - \alpha$ variation which occurs at larger *Re*. For $AR = 0.2$ and $\alpha \geq 30^\circ$, Fig. 8b in close-up, highlights the apparent discrepancies between the predicted Re_s and those reported by Dennis and Young (2003).

7.4 Variation of the bubble parameters with Re

Figures 9(a,b) show the variation of bubble length with *Re* for symmetric elliptic cylinders of aspect ratios ranging from 0.2 to 1. For each *AR*, it is observed that

the bubble elongates approximately linearly with increasing Re. This is a well known property of the steady separation bubble for a circular cylinder ($AR = 1$). Snowden (1967) conducted experiments on various bluff objects including the circular cylinder as well as flat plate. For all geometries, he observed linear $L - Re$ variation. The earlier studies on symmetric elliptic cylinders (Masliyah and Epstein (1971); Sivakumar, Bharti and Chhabra (2007)) however, do not comment on the linearity of L with Re. The best linear fit, using the least squares approximation, for various AR, are non-parallel (Fig. 9).

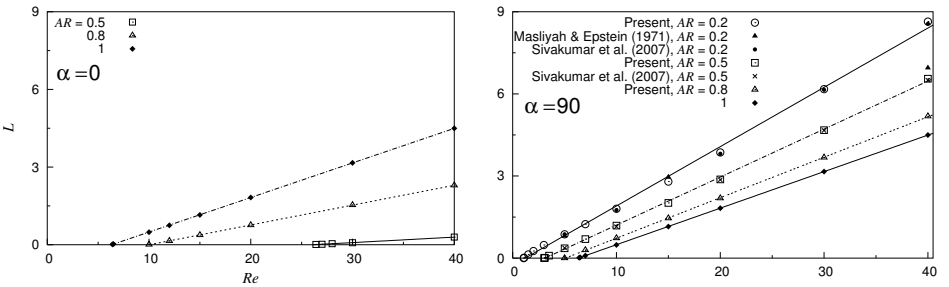

Figure 9: Steady separated flow past symmetric elliptic cylinders of $AR = 0.2$, 0.5, 0.8 and 1 in the unbounded medium: variation of bubble length, L with Re for $\alpha =$ (a) 0° and (b) 90°.

The value of L predicted at a fixed Re for 0° oriented cylinders decreases with decreasing AR. Conversely, significant rise in L is realized when the cylinders are oriented normal to the free-stream (see Fig. 9b). Also, the predicted bubble length increases manifold when a cylinder ($AR \neq 1$) is positioned normal to the x axis, than when it is aligned. The bubble lengths predicted for the cylinders of $AR = 0.2$ and 0.5 with $\alpha = 90^\circ$ compare favourably with those reported by Sivakumar, Bharti and Chhabra (2007). At $Re = 5$ and 15, the bubble length values predicted by Masliyah and Epstein (1971) for the perpendicularly oriented cylinder of $AR = 0.2$ are in excellent agreement with the current predictions. However, the value of L reported by Masliyah and Epstein (1971) at $Re = 40$ is significantly smaller than the current prediction, the deviation being about 20%. The present study as well as the one by Sivakumar, Bharti and Chhabra (2007) for $AR = 0.2$ and $\alpha = 90^\circ$, predict a bubble length that exceeds 8 times the length of semi-major axis. Fig. 7f of the paper by Dennis and Young (2003) for $\alpha = 90^\circ$ (or the second column of Fig. 6 in the present paper for the same configuration), indicates that the bubble length is about 6 times the length of semi-major axis. This suggests an underprediction of L by Dennis and Young (2003).

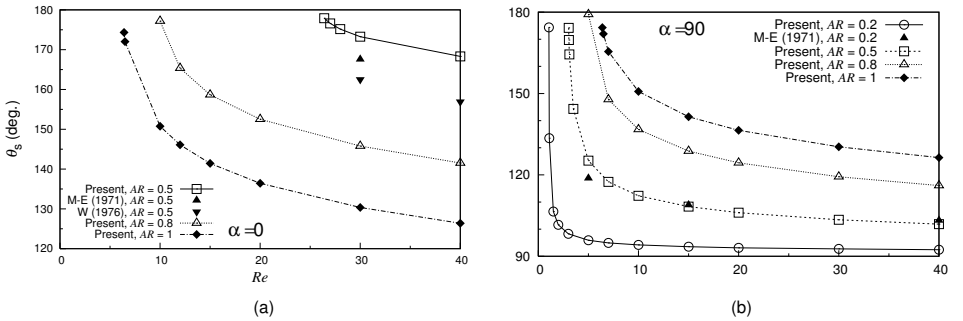

Figure 10: Steady separated flow past symmetric elliptic cylinders of $AR = 0.2$, 0.5, 0.8 and 1 in the unbounded medium: variation of the separation angle, θ_s with Re for $\alpha =$ (a) 0° and (b) 90°. The abbreviations used are: M-E, Masliyah and Epstein (1971) and W, Weinbaum, Kolansky, Gluckman and Pfeffer (1976).

For the symmetric cylinders of various thickness, Figs. 10a and 10b show the separation angle as a function of Re for $\alpha = 0^\circ$ and 90°, respectively. For each AR and α, the separation point moves upstream with increasing Re implying a decrease in θ_s. However, the decay in θ_s is non-linear. Near the onset of separation, the $\theta_s - Re$ curves are steep (particularly, for $\alpha = 90^\circ$) and the slope decreases with increasing Re. The separation angle, at a given Re, decreases for $\alpha = 0^\circ$ with increasing AR. It increases with increasing AR for $\alpha = 90^\circ$. Also, at constant Re, θ_s for a non-circular cylinder at $\alpha = 90^\circ$ is always smaller than its value at $\alpha = 0^\circ$. Fig. 10 clearly indicates that regardless of AR and α, the steady separation initiates from the base point of a symmetric cylinder, i.e. $\theta_s = 180^\circ$. Though close agreement with the results of Masliyah and Epstein (1971) for the predicted bubble length of $AR = 0.2$ cylinder for $\alpha = 90^\circ$ is observed at $Re = 5$ and 15, significant discrepancies in the values of predicted θ_s for $Re = 5$, 15 and 40 are quite apparent from Fig. 10b. Large discrepancies in the predicted separation angle are found with the values reported by Weinbaum, Kolansky, Gluckman and Pfeffer (1976) for the $AR = 0.5$ cylinder at $\alpha = 0^\circ$ (Fig. 10a). The smaller θ_s predicted by Weinbaum, Kolansky, Gluckman and Pfeffer (1976) also suggest for a much lower value (< 20) of Re_s (Fig. 11 of their paper) than the presently predicted value of 25.88 (see Tab. 6). At $Re = 30$, θ_s predicted by Masliyah and Epstein (1971) for the $AR = 0.5$ cylinder oriented at $\alpha = 0^\circ$ is smaller than the currently predicted value.

The variation of location of initial separation (θ_s at Re_s) for elliptic cylinders of various thickness and orientation is shown in Fig. 11. An important conclusion drawn from the figure is that the asymmetric separation initiates neither from the base point (trailing tip) nor the center ($\theta = 180^\circ$) of a cylinder. This is a contrasting

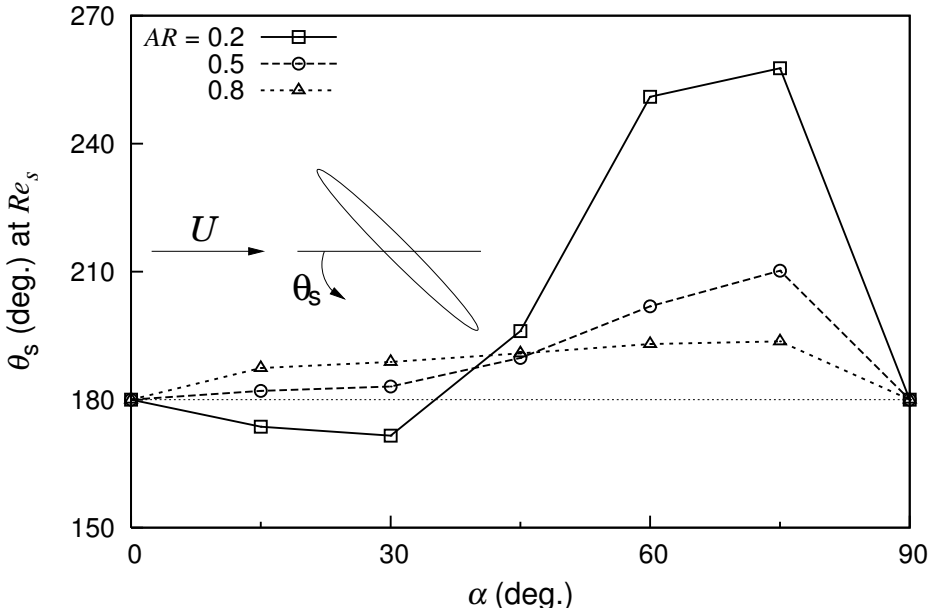

Figure 11: Steady separated flow past elliptic cylinders of AR = 0.2, 0.5 and 0.8 for $\alpha = 0^\circ - 90^\circ$ in the unbounded medium: variation of the location of initial separation at Re_s with α.

feature of asymmetric separation relative to the flow separation phenomenon for symmetric cylinders where flow separates invariably from the base point. The location of initial separation for the thick cylinder is practically insensitive to α. For each orientation it is found that the attached bubble forms little above the center or $\theta = 180^\circ$ location. When $\alpha \leq 30^\circ$, the bubble appears slightly above $\theta = 180^\circ$ for $AR = 0.5$ and increases with increasing α. Strong sensitivity of the location of bubble formation to α is seen for the thin cylinder. The flow separates near the trailing edge for $\alpha = 15^\circ$. The separation location travels non-monotonically towards the leading edge as α increases. An interesting observation from the figure is the apparent independence of the separation location on cylinder shape for $\alpha = 45^\circ$.

The variation of the separation (via point S) and attachment (via point R) angles of the bubble measured counterclockwise relative to the negative x axis, with Re is shown in Fig. 12. The movement of the separation-attachment points is nonlinear. For each α, the separation point travels towards the leading edge and the reattachment point towards the trailing tip in general.

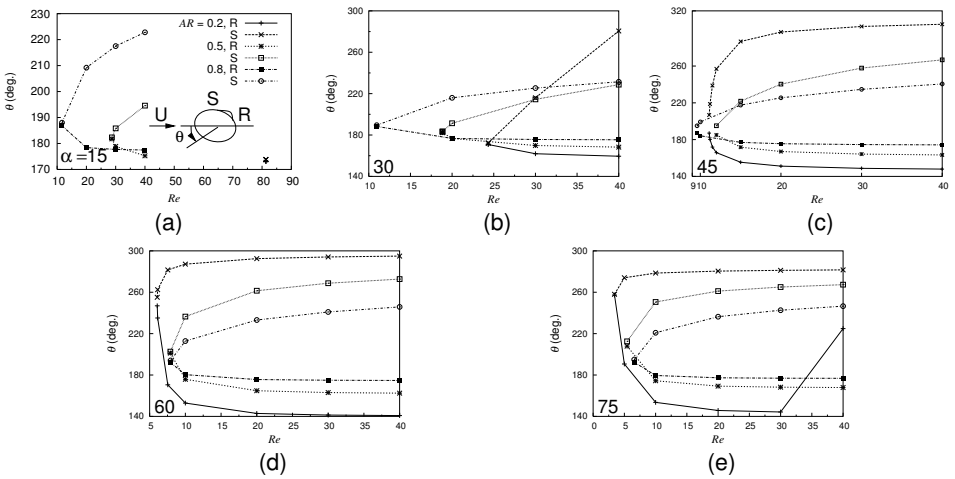

Figure 12: Steady separated flow past inclined elliptic cylinders of $AR = 0.2 - 0.8$: variation of the separation and reattachment angles of the attached bubble with *Re* for $\alpha =$ (a) 15°, (b) 30°, (c) 45°, (d) 60° and (e) 75°. S and R denote the separation and attachment points, respectively.

8 Conclusions

A stabilized finite-element method has been employed to investigate the steady, laminar flow around stationary elliptic cylinders at various angles of attack. The aspect ratios studied are 0.2, 0.5, 0.8 and 1.0. Results have been presented for $Re \leq 40$ and $0° \leq \alpha \leq 90°$. The separation of laminar boundary layer from symmetric cylinders of different *AR* initiates from the base point. The asymmetric separation however, does not initiate from the base point or center. For a thin cylinder at low incidence, the separation bubble forms near the trailing tip and with increasing α, the location of initial separation moves non-monotonically towards the leading tip. For thick cylinders, the effect of α on the location of initial separation is however, insignificant. The bubble appears for all α, slightly above the cylinder center. With increasing *Re*, the separation points of a symmetric cylinder advance upstream while for an asymmetric cylinder, the separation point moves towards the leading edge and the reattachment point towards the trailing edge in general. The wake topology is proposed for the asymmetric separation and differences in wake topology with the earlier predictions (Smith (1983); Dennis and Young (2003)) are pointed out. The developed wake for asymmetric separation is 'open' and contains one upper attached and lower (counterrotating) unattached eddy. This is in stark contrast with the postulates of Smith (1983) who proposed 'closed' wake at large

α and alternately, a single dominant eddy. The results presented by Dennis and Young (2003) suggest a lower attached and upper unattached eddy for $\alpha > 57^\circ$ and both eddies attached at $\alpha \approx 57^\circ$. Both these features are in contradiction with our proposed topology. We infer that a closed wake with two attached eddies is characteristic of separation for limiting values of α, i.e. 0° and 90°. The attached bubble for asymmetric separation appears at Re_s and contains only one recirculation zone while the isolated eddy appears at an Re exceeding the Re_s. This is a fundamental difference with respect to the symmetric separation where the attached wake bubble is closed and consists of two recirculation zones that appear at Re_s. Regardless of the AR, the separation bubble of symmetric elliptic cylinders elongates approximately linearly with Re. For $\alpha = 90^\circ$, the predicted bubble length is much larger and separation angle much smaller than the values obtained with $\alpha = 0^\circ$. For the symmetric cylinders, the bubble length criterion is utilized to determine Re_s. The predicted values of the onset Re are in very good agreement with those obtained by using the criterion proposed by Srinivasan (2006). For elliptic cylinders with major axis normal to the flow, Re_s decreases with decreasing AR. The surface vorticity distribution is utilized to determine Re_s for the asymmetric elliptic cylinders. For the first time, it is observed that Re_s for the elliptic cylinders of various thicknesses displays a non-monotonic dependence on α. At small α, Re_s initially increases and then decreases as α approaches 90°. For $\alpha < 45^\circ$, Re_s increases with decreasing AR and when $\alpha > 60^\circ$, the trend reverses.

References

Alben, S. (2008): An implicit method for coupled flow-body dynamics. *J. Comput. Phys.*, vol. 227, pp. 4912–4933.

Aref, H.; Brøns, M.; Stremler, M. A. (2007): Bifurcation and instability problems in vortex wakes. *Journal of Physics: Conference Series*, vol. 64, doi:10.1088/1742-6596/64/1/012015.

Batchelor, G. K. (1967): An introduction to fluid dynamics. *Cambridge University Press*.

Brøns, M.; Jakobsen, B.; Niss, K.; Bisgaard, A. V; Voigt, L. K. (2007): Streamline topology in the near wake of a circular cylinder at moderate Reynolds numbers. *J. Fluid Mech.*, vol. 584, pp. 23–43.

Brooks, A. N.; Hughes, T. J. R. (1982): Streamline upwind/Petrov-Galerkin formulations for convection dominated flows with particular emphasis on the incompressible Navier-Stokes equations.. *Comput. Methods Appl. Mech. Eng.*, vol. 32, pp. 199–259.

Coutanceau, M.; Bouard, R. (1977): Experimental determination of the main features of the viscous flow in the wake of a circular cylinder in uniform translation. Part 1. Steady flow. *J. Fluid Mech.*, vol. 79, pp. 231–256.

D'Alessio S. J. D.; Dennis, S. C. R. (1994): A vorticity model for viscous flow past a cylinder. *Comput. Fluids*, vol. 23, pp. 279–293.

Dennis, S. C. R.; Chang, G. Z. (1969): Numerical integration of the Navier-Stokes equations for steady two-dimensional flows. *Phys. Fluids Suppl.*, vol. 12, pp. II 88–II 93.

Dennis, S. C. R.; Chang, G. Z. (1970): Numerical solutions for steady flow past a circular cylinder at Reynolds numbers up to 100. *J. Fluid Mech.*, vol. 42, pp. 471–489.

Dennis, S. C. R.; Young, P. J. S. (2003): Steady flow past an elliptic cylinder inclined to the stream. *J. Eng. Math.*, vol. 47, pp. 101–120.

Faruquee, Z.; Ting, D. S-K.; Fartaj, A.; Barron, R. M.; Carriveau, R. (2007): The effects of axis ratio on laminar fluid flow around an elliptic cylinder. *Int. J. Heat Fluid Flow*, vol. 28, pp. 1178–1189.

Hughes, T. J. R.; Brooks, A. N. (1979): A multi-dimensional upwind scheme with no crosswind diffusion. *Finite Element Methods for Convection Dominated Flows (ed. T. J. R. Hughes)*, vol. 47, pp. 19–35.

Hughes, T. J. R.; Franca, L. P.; Balestra, M. (1979): A new finite element formulation for computational fluid dynamics: V. Circumventing the Babuška-Brezzi condition: A stable Petrov-Galerkin formulation of the Stokes problem accommodating equal-order interpolations. *Comput. Methods Appl. Mech. Eng.*, vol. 59, pp. 85–99.

Imai, I. (1954): A new method of solving Oseen's equations and its application to the flow past an inclined elliptic cylinder. *Proc. R. Soc. Lond. A*, vol. 224, pp. 141–160.

Khan, W. A.; Culham, J. R.; Yovanovich, M. M. (2005): Fluid flow around and heat transfer from elliptical cylinders: analytical approach. *J. Thermophysics Heat Transfer*, vol. 19, pp. 178–185.

Lighthill, M. J. (1963): Boundary layer theory. *Laminar boundary layers (ed. L. Rosenhead), Oxford University Press*, pp. 46–103.

Lugt, H. J.; Haussling, H. J. (1974): Laminar flow past an abruptly accelerated elliptic cylinder at 45° incidence. *J. Fluid Mech.*, vol. 65, pp. 711–734.

Masliyah, J. H.; Epstein, N. (1971): Steady symmetric flow past elliptic cylinders. *Ind. Eng. Chem. Fundam.*, vol. 10, pp. 293–299.

Park, J. K.; Park, S. O.; Hyun, J. M. (1989): Flow regimes of unsteady laminar flow past a slender elliptic at incidence. *Int. J. Heat Fluid Flow*, vol. 10, pp. 311–317.

Perry, A. E.; Chong, M. S.; Lim, T. T. (1982): The vortex-shedding process behind two-dimensional bluff bodies. *J. Fluid Mech.*, vol. 116, pp. 77–90.

Pruppacher, H. R.; Clair, B. P. Le; Hamielec, A. E. (1970): Some relations between drag and flow past a sphere and a cylinder at low and intermediate Reynolds numbers. *J. Fluid Mech.*, vol. 44, pp. 781–790.

Saad, Y.; Schultz, M. (1986): GMRES: A generalised minimal residual algorithm for solving nonsymmetric linear systems. *SIAM J. Sci. Stat. Comput.*, vol. 7, pp. 856–869.

Sahin, M.; Owens, R. G. (2004): A numerical investigation of wall effects up to high blockage ratios on two-dimensional flow past a confined circular cylinder. *Phys. Fluids*, vol. 16, pp. 1305–1320.

Sen, S. (2010): Flow past stationary and vibrating cylinders of various cross-sections at low Reynolds numbers. *PhD Thesis, Indian Institute of Technology Kanpur*.

Sen, S.; Mittal, S.; Biswas, G. (2009): Steady separated flow past a circular cylinder at low Reynolds numbers. *J. Fluid Mech.*, vol. 620, pp. 89–119.

Sen, S.; Mittal, S.; Biswas, G. (2011): Flow past a square cylinder at low Reynolds numbers. *Int. J. Num. Methods Fluids*, vol. 67, pp. 1160–1174.

Shintani, K.; Umemura, A.; Takano, A. (1983): Low-Reynolds-number flow past an elliptic cylinder. *J. Fluid Mech.*, vol. 136, pp. 277–289.

Sivakumar, P.; Bharti, R. P.; Chhabra, R. P. (2007): Steady flow of power-law fluids across an unconfined elliptic cylinder. *Chem. Eng. Sci.*, vol. 62, pp. 1682–1702.

Smith, F. T. (1983): Interacting flow theory and trailing edge separation − no stall. *J. Fluid Mech.*, vol. 131, pp. 219–249.

Snowden, D. D. (1967): The steady separated flow past bluff objects. *Ph.D. Thesis, Stanford University*.

Srinivasan, K. (2006): On a separation criterion for symmetric elliptic bluff body flows. *http://arxiv.org/pdf/physics/0511250*.

Sugihara-Seki, M. (1993): The motion of an elliptic cylinder in channel flow at low Reynolds numbers. *J. Fluid Mech.*, vol. 257, pp. 575–596.

Taneda, S. (1956a): Experimental investigation of the wakes behind cylinders and plates at low Reynolds numbers. *J. Phys. Soc. Japan*, vol. 11, pp. 302–307.

Taneda, S. (1956b): Experimental investigation of the wake behind a sphere at low Reynolds numbers. *J. Phys. Soc. Japan*, vol. 11, pp. 1104–1108.

Tezduyar, T. E.; Mittal, S.; Ray, S. E.; Shih, R. (1992): Incompressible flow computations with stabilized bilinear and linear equal-order-interpolation velocity-pressure elements. *Comput. Methods Appl. Mech. Eng.*, vol. 95, pp. 221–242.

Tomotika, S.; Aoi, T. (1953): The steady flow of a viscous fluid past an elliptic cylinder and a flat plate at small Reynolds numbers. *Q. J. Mech. Appl. Math.*, vol. 6, pp. 290–312.

Weinbaum, W.; Kolansky, M. S.; Gluckman, M. J.; Pfeffer, R. (1976): An approximate theory for incompressible viscous flow past two-dimensional bluff bodies in the intermediate Reynolds number regime O(1)$<$ *Re* $<$O(10^2). *J. Fluid Mech.*, vol. 77, pp. 129–152.

Yano, H.; Kieda, A. (1980): An approximate method for solving two-dimensional low-Reynolds-number flow past arbitrary cylindrical bodies. *J. Fluid Mech.*, vol. 97, pp. 157–179.